In Vitro Uterine Strain Imaging

Preliminary Results

Maritza A. Hobson, MS, Miklos Z. Kiss, PhD, Tomy Varghese, PhD, Amy M. Sommer, MS, Mark A. Kliewer, MD, James A. Zagzebski, PhD, Timothy J. Hall, PhD, Josephine Harter, MD, Ellen M. Hartenbach, MD, Ernest L. Madsen, PhD

Objective. Uterine abnormalities, such as leiomyomas, endometrial polyps, and adenomyosis, are often clinically associated with irregular uterine bleeding. These abnormalities can have similar B-mode characteristics but require different treatment. The objective of this study was to develop diagnostic techniques based on ultrasound strain imaging that would allow in vivo visualization and characterization of endometrial and myometrial uterine abnormalities, enabling physicians to improve diagnosis and treatment. ***Methods.*** Ultrasound strain imaging was performed on 29 uteri removed via elective hysterectomy. An ultrasound system with a linear array transducer was used to obtain radio frequency echo data during manual freehand compressions of the tissue. Radio frequency data were post-processed with a 2-dimensional block-matching algorithm to generate strain images. ***Results.*** In the uteri involved in this study, there were 19 leiomyomas, 1 case of adenomyosis, and 3 endometrial polyps observed on strain imaging. Leiomyomas appeared stiffer than the surrounding normal myometrium in strain images and were characterized by a slipping artifact at their boundary. Endometrial polyps appeared softer than the normal surrounding myometrium. The average strain contrast in small leiomyomas (<1.5 cm) compared to the myometrium was 1.75 ± 1.14; the strain contrast was 2.50 ± 1.15 in large leiomyomas and 0.40 ± 0.05 in endometrial polyps. Leiomyoma strain contrast results were consistent with modulus contrast values from mechanical testing results. ***Conclusions.*** Ultrasound strain imaging can differentiate between endometrial polyps and leiomyomas. More data are necessary to validate these results and to ascertain whether other uterine abnormalities can also be differentiated. ***Key words:*** adenomyosis; elastography; endometrial polyps; leiomyomas; strain imaging; uterus.

Abbreviations
MRI, magnetic resonance imaging; RF, radio frequency; 2D, 2-dimensional

Received January 4, 2007, from the Departments of Medical Physics (M.A.H., M.Z.K., T.V., A.M.S., J.A.Z., T.J.H., E.L.M.), Radiology (M.A.K.), Pathology (J.H.), and Obstetrics and Gynecology (E.M.H.), University of Wisconsin–Madison, Madison, Wisconsin USA. Dr Kiss is currently with Volcano Corp, Cleveland, Ohio USA. Revision requested February 13, 2007. Revised manuscript accepted for publication February 28, 2007.

We thank Jingfeng Jiang, PhD, for help in data processing for the strain images; Shyam Bharat, Hao Chen, Lee Kiessel, Matthew McCormick, Min Rao, and Hairong Shi for help in radio frequency data collection; and the Surgical Pathology Laboratory staff for help during radio frequency data collection. This study was funded in part by National Institutes of Health grants R01EB000459, R01CA100373, and 2-T32-CA-09206 and received technical support from Siemens Medical Solutions USA, Inc, Ultrasound Division (Mountain View, CA).

Address correspondence to Maritza A. Hobson, MS, Department of Medical Physics, University of Wisconsin–Madison, 1300 University Ave, 1530 MSC, Madison, WI 53706 USA.

E-mail: mahobson@gmail.com

Uterine abnormalities tend to be clinically evident as dysfunctional uterine bleeding. Although most cases result from a benign etiology, approximately 10% to 30% of women with dysfunctional uterine bleeding will be found to have endometrial cancer.[1]

Three of the benign causes of dysfunctional uterine bleeding are leiomyomas (uterine fibroids), endometrial polyps, and adenomyosis. Leiomyomas are stiff growths of homogeneous tissue bundles of smooth muscle and can be differentiated from the normal myometrium by the presence of a capsule.[2–4] Submucosal leiomyomas that project into the uterine cavity are thought to cause dysfunctional uterine bleeding because they usually expand the endometrial surface and disturb the regular shedding process.[5] Adenomyosis is a condition in which the soft endometrial glands, smooth muscle cells, and stroma invade the myometrium, creating cysts in the tissue, and usually affects the posterior wall of the uterus.[4,6]

Endometrial polyps are focal hyperplastic growths of the endometrial glands and stroma, which may contain malignant cells.[7]

Ultrasound B-mode characteristics of leiomyomas, endometrial polyps, and adenomyosis can be compared to the surrounding normal uterine tissue. Compared to the myometrium, the basal layer of the endometrium is hyperechoic due to the specular reflections from the ramifying glands, whereas the functional layer of the endometrium is hypoechoic compared to the basal layer.[8] Submucosal leiomyomas are usually hypoechoic compared to the myometrium,[4,5,9] but as they become more heterogeneous due to the presence of degeneration, calcification, or necrosis, the heterogeneity of the echo structure also increases.[10] When heterogeneous leiomyomas are present, it can be difficult to distinguish them from endometrial polyps, adenomyosis, blood, or mucus. Typical endometrial polyps are hyperechoic compared to the myometrium and isoechoic to the endometrium with a homogeneous echo texture.[7,11] In transvaginal ultrasound images, adenomyosis appears as a hypoechoic region in the myometrium.[10,12]

For premenopausal women, dysfunctional uterine bleeding most often results from leiomyomas, endometrial polyps, and adenomyosis. These may have similar appearances on B-mode ultrasound scans, which can make differentiating between the conditions problematic with conventional ultrasound techniques, especially when there are diffuse echo texture changes.[10,12] This differentiation, however, is clinically important because treatment for the 3 conditions differs considerably. Currently, magnetic resonance imaging (MRI) is widely accepted as the most capable modality for distinguishing between adenomyosis and leiomyomas.[13,14] However, MRI studies are expensive and may be unavailable to some patients, preventing MRI from being a first choice for screening the large number of patients with dysfunctional bleeding.

For postmenopausal women, the main causes of dysfunctional uterine bleeding are endometrial polyps, endometrial cancer, endometrial hyperplasia (or atrophy), and leiomyomas.[4] Endometrial cancer shares a symptom of abnormal uterine bleeding with benign conditions.[1,13,15] Endometrial biopsies are generally used to diagnose endometrial cancer because they sample a significant portion of the endometrial lining.[16] However, current diagnostic techniques, including endometrial biopsy, do not allow differentiation between other sources of dysfunctional uterine bleeding, especially when more than 1 of these conditions is present.

Due to the differences in their tissue orientation and makeup, the treatment options vary for leiomyomas, endometrial polyps, and adenomyosis.[3,5,11,12,17–19] Thus, finding a way to accurately diagnose the causes for abnormal uterine bleeding in vivo would allow the physician to decide on appropriate treatment methods to avoid unnecessary hysterectomies. Manual palpation is a form of diagnosis that has been used for centuries to differentiate between normal and abnormal conditions. However, palpation does not provide quantitative information that can be compared from one patient visit to the physician to the next and often cannot be easily performed on organs such as the uterus.

Two imaging modalities, ultrasound strain imaging[20–23] and magnetic resonance elastography,[24–29] are being investigated for providing a more quantitative approach to palpation of organs accessible and inaccessible to manual palpation. Both modalities image the strain or stiffness distribution throughout an organ in response to an applied stress. Due to the differences in tissue makeup and stiffness between adenomyosis, endometrial polyps, and leiomyomas, ultrasound strain imaging may have the potential to provide additional diagnostic information by differentiating between these 3 conditions. In this article, we present preliminary results that illustrate the ability of in vitro ultrasound strain imaging to differentiate between leiomyomas and endometrial polyps on excised intact human uteri.

Materials and Methods

Ultrasound strain imaging was performed on uteri removed via elective hysterectomy at the University of Wisconsin–Madison Hospitals and Clinics. Most of these surgeries were precautionary or preventive hysterectomies in women who had no known uterine cancer or other serious uterine pathology issues. Patient consent for the

strain imaging study was obtained before surgery, and all postsurgical imaging was performed under a protocol approved by the University of Wisconsin–Madison Hospitals and Clinics Institutional Review Board. The study was also compliant with the Health Insurance Portability and Accountability Act. Tissue was obtained from 29 patients ranging in age from 32 to 84 years (mean age, 54.5 years; SD, 13.2 years). Histopathology results on the excised uteri are summarized in Table 1.

Table 1. Summary of Histopathology Results of the Number of Patients With a Certain Condition or Lesion and the Number of That Lesion or Condition Observed in This Study

Condition	No. of Patients	No. of Lesions/Conditions Observed
Normal	4	NA
Leiomyomas (fibroids)	21	19
Adenomyosis	1	1
Endometrial polyps	6	3

NA indicates not applicable.

Ultrasound radio frequency (RF) data sets were acquired on all 29 uteri within 30 minutes of excision. Data were collected with the Ultrasound Research Interface on a SONOLINE Antares system (Siemens Medical Solutions USA, Inc, Ultrasound Division, Mountain View, CA) with a VFX 13-5 linear array transducer. The transducer was excited with an 11.4-MHz pulse, and the transmitted signal had an approximately 80% bandwidth. Digitized RF echo data were sampled at 40 MHz and stored for offline processing. Freehand palpation using the transducer was applied to the excised uteri as the mechanical stimulus for strain imaging.[21] To determine the areas for RF data acquisition, the transducer was systematically scanned along the cranial-caudal direction to find lesions within the uterus. Radio frequency data were acquired where lesions were evident on B-mode imaging. Otherwise, RF data were acquired on the myometrium and cervix.

Offline analysis of the RF data sets consisted of up-sampling in the axial direction 4 times using a filter-based 2-dimensional (2D) spline interpolator. Strain images were produced by applying a modified 2D block-matching algorithm with a 2D search strategy[30] to estimate displacement with relatively large frame average strain (1%-2% for in vitro uterine tissue). The 2D block-matching algorithm computed the sum-squared difference between precompression and postcompression RF frames for a rectangular kernel. The motion-tracking kernel size was 1.0×0.3 mm^2 (width × length) with a 50% overlap between adjacent tracking kernels. Linear regression with a sliding 2.43-mm window was used to estimate the axial strain from these displacement estimates. In real-time imaging, there is a fixed temporal relationship between the precompression and postcompression echo fields. In post-processing, which takes up to 30 minutes per RF data set, the pairing of the precompression and postcompression data can be dynamically adjusted to achieve a nominal frame average strain of 0.8% to 1.2% to obtain high–signal-to-noise ratio strain images.[30]

After completion of freehand strain imaging, the uterine specimen was sliced, and 1-cm^3 specimens of the normal myometrium, cervix, and leiomyomas, if available, were used for dynamic mechanical testing of the uterine samples. Dynamic testing was performed from 0.1 to 100 Hz on excised tissue samples with an EnduraTEC 3200 ElectroForce system (Bose Corporation, ElectroForce Systems Group, Eden Prairie, MN), and these results were presented by Kiss et al.[31] Histopathology analysis was done on these samples, and the results were compared to the axial strain elastogram. Due to the need for immediate pathology reports, we were unable to use endometrial polyps for dynamic testing. It should also be noted that the exact leiomyoma from which the tissue sample was taken from patients with multiple leiomyomas was not known. Thus, there was no spatial correlation done between the strain images and the dynamic testing and pathology results, and correlation between lesion size in the strain image and pathology results could not be reported.

Results

Figures 1–7 show B-mode images on the top and strain images on the bottom from different patients with varying uterine pathologies. In each B-mode image, a white rectangular box outlines the region of interest for strain image formation. In these strain images, regions of

higher tissue strain appear brighter on the gray scale, whereas regions of lower strain appear darker. Arrows and arrowheads have been placed exactly in the same exact locations on the strain and B-mode image pairs (allowing direct comparison). The arrows were used to mark the edges of the leiomyomas and endometrial polyps, and the arrowheads were used to mark the slipping artifacts in Figure 1 and the endometrial lining in Figures 3–5.

Leiomyomas

Figures 1–5 illustrate B-mode and strain images of leiomyomas from different study patients. All lesions that are stiffer than the background myometrium are visualized on the strain images. These include all the lesions identified as leiomyomas from the B-mode images and pathology. In all the strain images of the leiomyomas, a clear delineation between the boundary of the leiomyoma and the normal surrounding myometrium

Figure 1. B-mode (**a**) and strain (**b**) images of a small leiomyoma from patient 12, a 32-year-old woman with 3 leiomyomas of 1.0, 3.5, and 5.5 cm in maximal direction without necrosis or hemorrhage. In the B-mode image, a white rectangular box outlines the region of interest for strain image formation. The edges of the leiomyoma are marked by arrows, and the slipping artifacts are marked by arrowheads. In the B-mode image, it is difficult to differentiate the leiomyoma from the surrounding normal myometrium. However, in the strain image, the slipping artifact may be used as a method of differentiation.

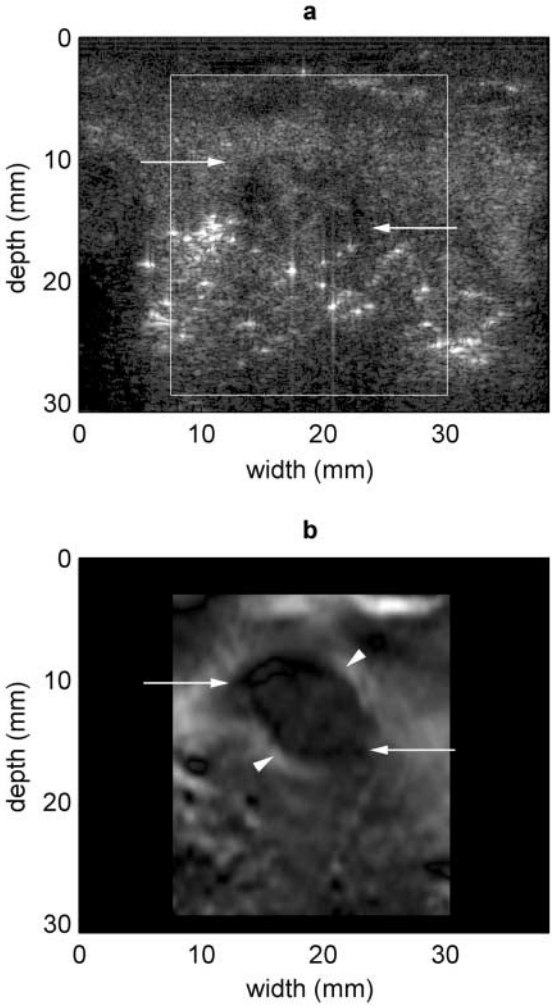

Figure 2. B-mode (**a**) and strain (**b**) images of a large leiomyoma from patient 14, a 51-year-old woman with 3 intramural leiomyomas with maximal dimension of 2.5 to 4.8 cm without areas of necrosis or hemorrhage. In the B-mode image, a white rectangular box outlines the region of interest for strain image formation. The edges of the leiomyoma are marked by arrows. In the B-mode image, it is difficult to distinguish the lower boundary of the leiomyoma due to shadowing. In the strain image, however, this boundary is evident due to the slipping artifact, the apparently brighter softer region surrounding the leiomyoma, marked by arrowheads.

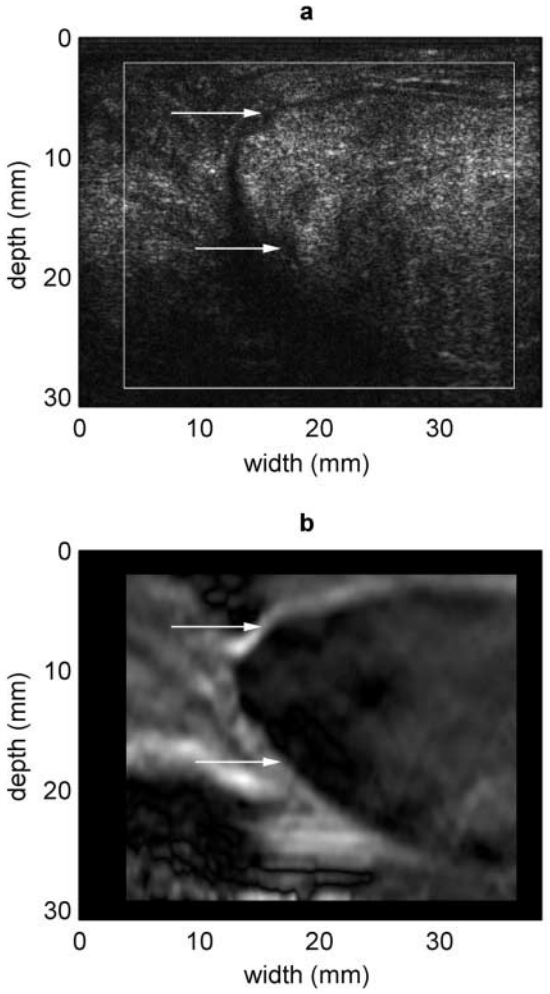

is observed. This delineation is significantly enhanced by the bright stripe (apparently softer region) around the entire leiomyoma, which is probably a slipping artifact induced at the capsule that characteristically surrounds uterine leiomyomas. This slipping artifact was noticed in all 24 RF data sets that included leiomyomas surrounded by myometrial tissue. From the RF data acquired, the smallest leiomyoma dimension observed on strain images was 8 mm. The largest leiomyoma that could be observed in strain images was limited by the field of view provided by the ultrasound transducer, and a number of the larger leiomyomas were bigger than the field of view.

Figure 2 provides an example of a larger leiomyoma, where in the B-mode image, a border between the normal myometrial tissue and the leiomyoma can be observed at the top of the image. However, it is difficult to distinguish the lower boundary of the leiomyoma in the B-mode images due to shadowing. In the strain image

Figure 3. B-mode (**a**) and strain (**b**) images of small leiomyomas from patient 27, a 47-year-old woman with the myometrium containing 10 tan-white, whorled apparent leiomyomas of 0.5 to 3.3 cm in maximal dimension and with no areas of necrosis or hemorrhage. In the B-mode image, a white rectangular box outlines the region of interest for strain image formation. The edges of the leiomyomas are marked by arrows, and the endometrial lining is marked by arrowheads. In the strain image, one can see a clear delineation of 1 leiomyoma on the left side from the myometrium as well as a clear delineation between the endometrial lining and the myometrium.

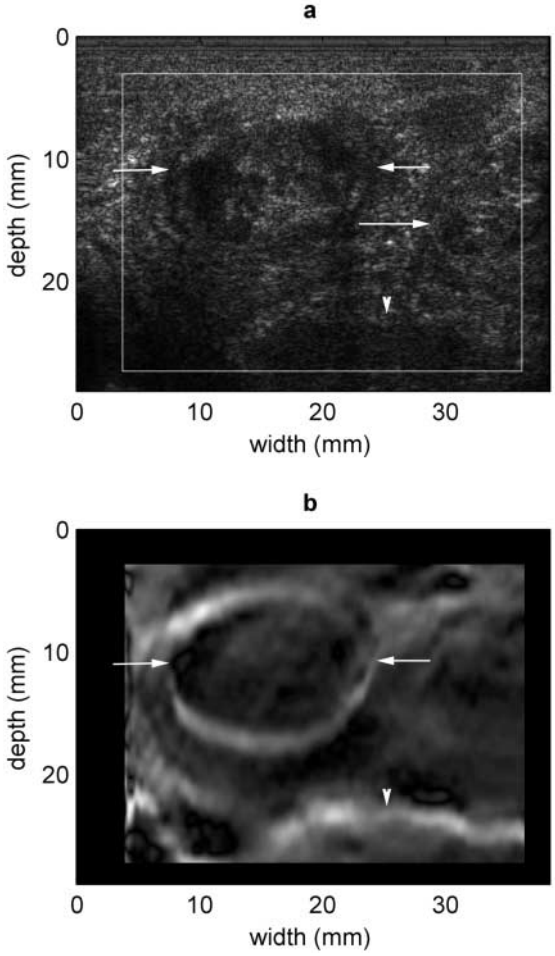

Figure 4. B-mode (**a**) and strain (**b**) images of a later frame from the same set of data shown in Figure 3 after additional compression. In the B-mode image, a white rectangular box outlines the region of interest for strain image formation. The edges of the leiomyomas are marked by arrows, and the endometrial lining is marked by arrowheads. The second leiomyoma on the right side of the strain image can be differentiated from the surrounding normal myometrium, and the size of the left leiomyoma has also changed. Both of these factors indicate elevational motion.

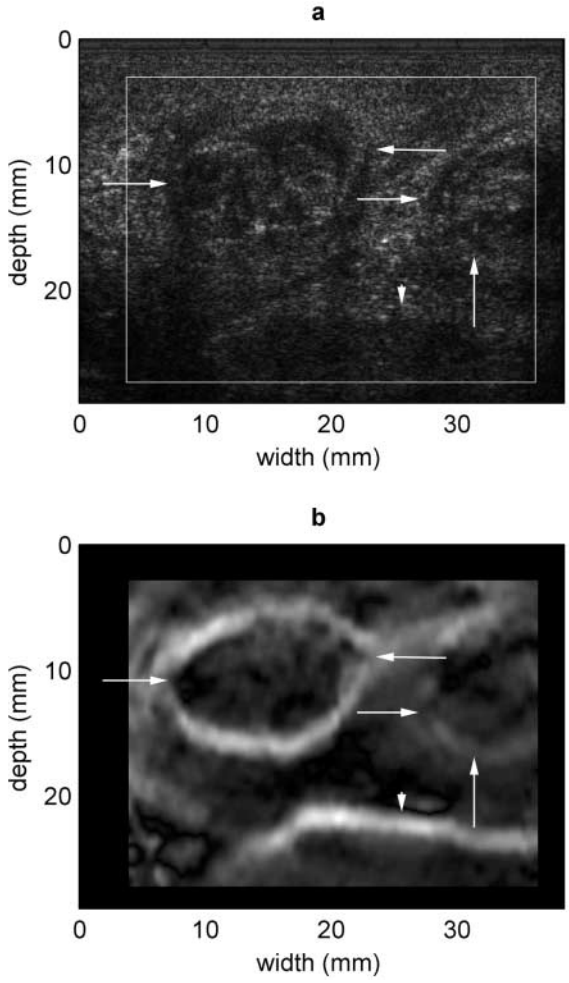

shown in Figure 2b, this border between the normal myometrium and leiomyoma is evident over the whole search region by the bright slipping artifact, the apparently softer region, surrounding the leiomyoma, as indicated by the arrows.

An example in which elevational motion likely compromised strain images is shown in Figures 3–5. Here, 3 different frames that depict leiomyomas from the uterus of a 47-year-old patient with 10 leiomyomas that ranged from 0.5 to 3.3 cm in maximal dimension are presented. Figure 3 is a strain image from the earliest frame in the RF loop, whereas Figures 4 and 5 are from later frames. In all 3 strain images, the softer endometrial lining appears at the bottom of the image, identified by an arrowhead, whereas the boundaries of the leiomyomas are shown with arrows. In Figure 3, one can see a clear delineation of 1 leiomyoma on the left side of the strain image. In Figures 4 and 5, after additional compression by the handheld transducer, the second leiomyoma on the right side of the strain image can be dif-

Figure 5. B-mode (**a**) and strain (**b**) images of a later frame from the same set of data shown in Figures 3 and 4 after additional compression. In the B-mode image, a white rectangular box outlines the region of interest for strain image formation. The edges of the leiomyomas are marked by arrows, and the endometrial lining is marked by arrowheads. The second leiomyoma on the right side can again be differentiated from the surrounding normal myometrium, and the size of the left leiomyoma has also changed again. Both of these factors indicate elevational motion.

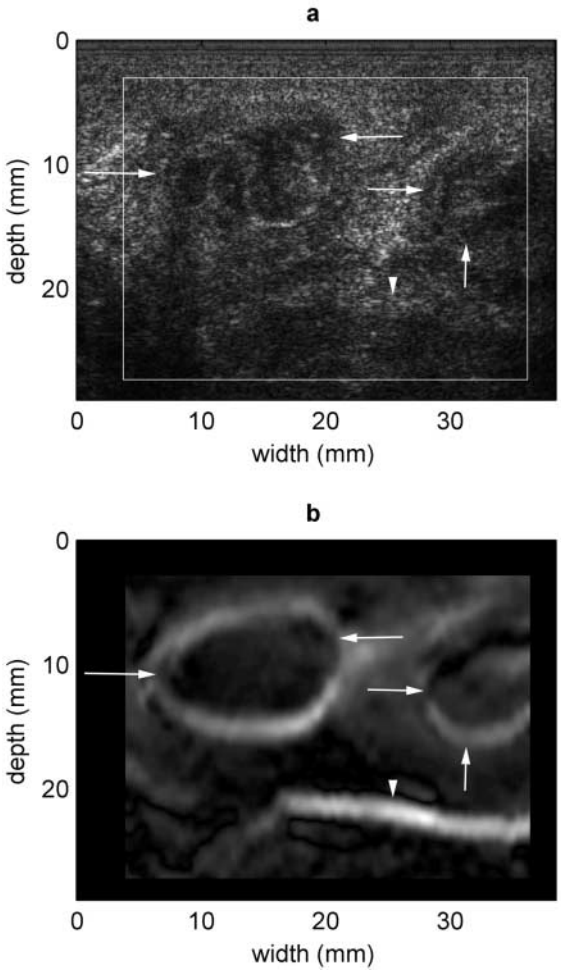

Figure 6. B-mode (**a**) and strain (**b**) images of endometrial polyps from patient 14, a 51-year-old woman with 2 endometrial polyps with dimensions of 1.1 × 0.9 × 0.6 and 1.2 × 0.5 × 0.3 cm^3. In the B-mode image, a white rectangular box outlines the region of interest for strain image formation. The edges of the endometrial polyps are marked by arrows. The endometrial polyp appears to be as soft as the endometrial lining. In the strain image, it is difficult to differentiate between the 2 polyps, but there is clearly a softer abnormality between the endometrial lining.

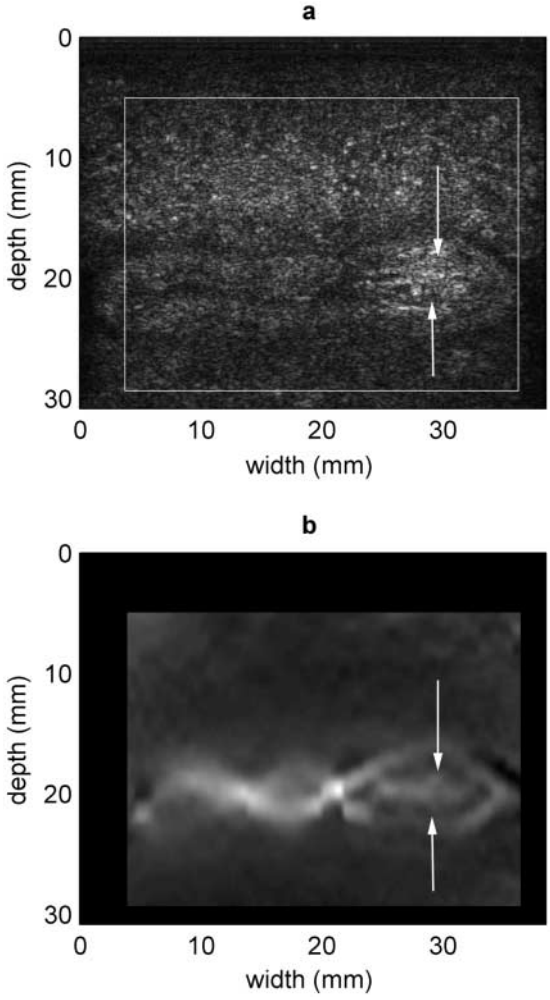

ferentiated from the surrounding normal myometrium. The size of the left leiomyoma in Figures 3–5 also changes over the time of acquisition, likely indicating the presence of elevational motion during compression of the uterus.

Endometrial Polyps

Figure 6 illustrates a strain image and B-mode image of an endometrial polyp. Observe in the image that the endometrial polyp, indicated by arrows, appears to be softer (brighter) than the surrounding myometrial tissue and appears to be as soft as the endometrial lining.

Adenomyosis

Only 1 patient in the study had a diagnosis of adenomyosis after pathology (Figure 7). The strain image in this case shows no clear delineation between the endometrium and the myometrium, which is seen in some of the previous figures from patients without adenomyosis (Figures 1 and 3–5). The strain image also indicates softer tissue regions in the myometrium in the top left region of the image that are not seen in the B-mode image.

Contrast in Strain Images

It is useful to study the strain contrast between leiomyomas, endometrial polyps, and other diffuse and focal masses and the normal myometrial tissue. Many of the patients in this study had large pedunculated, serosal, or subserosal leiomyomas that allowed imaging of the leiomyoma but not the leiomyoma and the myometrium simultaneously. Thus, strain contrast could only be calculated for a few of the patients from the patient population imaged.

The definition of strain contrast was as follows:

$$\text{strain contrast} \equiv \frac{\text{strain in background}}{\text{strain in lesion}},$$

where the lesion was either the endometrial polyp or uterine leiomyoma, and the background was the surrounding normal myometrial tissue. The strain contrast was defined in this manner, that is, using the mean strain of the lesions in the denominator, to allow a direct comparison of the strain contrast with the modulus contrast. Otherwise, the strain contrast would have an inverse relationship with the modulus contrast. The strain contrast was determined by selecting a sequence of at least 3 consecutive strain images that depicted the leiomyoma from an RF data set. In each frame, a region of interest was chosen within the leiomyoma or endometrial polyp in which there were no artifacts present, and the mean strain and the strain SD were calculated. For the endometrial polyps, the areas of high strain were selected to calculate the strain contrast. The same was done for the surrounding normal myometrial tissue, and from these values, the mean strain contrast was determined for that RF sequence.

Figure 7. B-mode (**a**) and strain (**b**) images of adenomyosis in patient 26, a 54-year-old woman with adenomyosis with an endometrial thickness of 0.2 cm. In the B-mode image, a white rectangular box outlines the region of interest for strain image formation. The strain image shows no clear delineation between the endometrium and the myometrium, which is shown in Figures 3–6. This implies the possibility of a thicker endometrium and growth of the endometrial tissue into the myometrium. The strain image also indicates softer tissue regions in the myometrium in the top left region of the image that are not seen in the B-mode image, which possibly correspond to cysts.

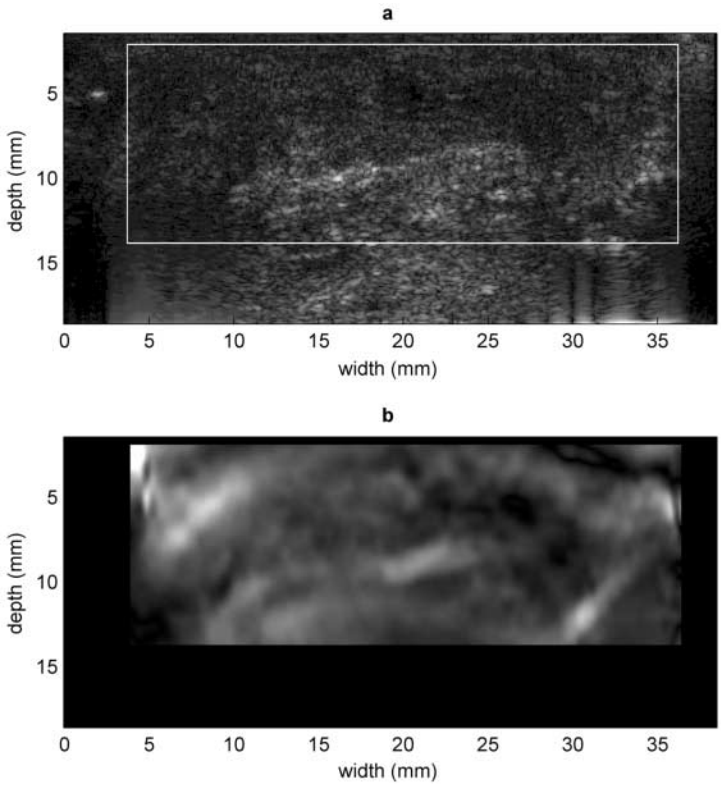

For analysis purposes, the lesions were broken into 3 different types: large leiomyomas, small leiomyomas, and endometrial polyps. A large leiomyoma took up most of the transducer field of view (ie, 40 mm or leiomyomas that were >1.5 cm), whereas a small leiomyoma was 0.8 to 1.5 cm in diameter. The average over all the data sets used for each lesion type is shown in Table 2.

Discussion

Leiomyomas

Similar instances of slipping artifacts have been reported in strain images of unbound lesions in an anthropomorphic breast phantom,[21] breast fibroadenomas,[32,33] and thyroid nodules.[31] This slipping artifact in strain images might be used as a method of differentiating a leiomyoma from the surrounding normal myometrium. This differentiation is difficult to accomplish in regular B-mode images due to shadowing, as shown in the B-mode image in Figure 1. However, it is very important to be able to determine the size and extent of leiomyomas because this information establishes the treatment method used.

Because leiomyomas are composed of stiff fibrotic tissue, hysteroscopic resection can be performed only on intracavitary parts of submucosal leiomyomas by carving parts of the leiomyoma off and removing them through the cervix.[11] This is usually only recommended if 50% of the leiomyoma is protruding into the endometrial cavity, as determined from diagnostic hysteroscopy, sonography, or MRI.[11] Thus, strain imaging can further improve the diagnostic capabilities of current B-mode imaging in the uterus by determining the extent and size of uterine leiomyomas when shadowing is present, as in Figure 2, and can help determine whether a hysteroscopic resection is possible.

The effect of elevational motion seen in Figures 3–5 emphasizes the importance of analyzing sequences of leiomyoma strain images because a single frame may give an incorrect fibroid maximum diameter. For example, if the fibroid is present in the B-mode image and not in the strain image, it may be incorrectly assumed that the strain in the fibroid is higher than expected, leading to potential misdiagnosis. Looking at more than 1 frame or a sequence of frames will allow the correct strain in the leiomyoma to be determined.

Endometrial Polyps

Endometrial polyps appearing to be as soft as the endometrial lining, as shown in Figure 6b, are expected because endometrial polyps are derived from the same type of tissue as the endometrial lining. It is difficult to differentiate between the 2 polyps in Figure 6b, but there is clearly a softer abnormality between the endometrial lining.

Adenomyosis

The lack of delineation between the endometrium and the myometrium seen in the 1 case of adenomyosis implies the possibility of a thicker endometrium (measured pathologically to be 0.2 cm thick) and the growth of endometrial tissue into the myometrium. However, the degree of adenomyosis in this patient is not known. The softer tissue regions in the myometrium in the top left region of the image possibly correspond to the characteristic cysts seen in adenomyosis. The importance of showing this 1 case of adenomyosis is to show that there are definite differences in strain distributions between adenomyosis and leiomyomas. Further testing on more patients with adenomyosis should allow more definite conclusions of the strain characteristics of adenomyosis.

Table 2. Mean and SD of the Strain Contrast Over All Patients for Small Leiomyomas, Large Leiomyomas, and Endometrial Polyps

Lesion Type	n*	No. of Lesions	Mean Age, y	Mean Strain Contrast
Small leiomyoma	64	5	42 ± 7	1.75 ± 1.14
Large leiomyoma	78	10	45 ± 7	2.50 ± 1.15
Endometrial polyp	24	3	48 ± 3	0.40 ± 0.05

*Number of frames used to calculate the values.

Contrast in Strain Images

The variability in the strain contrast, especially in the small and large leiomyomas, could be due to the internal histology content and is being investigated. However, none of the leiomyomas in this study had any signs of necrosis or hemorrhage.

The generalization that can be made from the results in Table 2 is that leiomyomas have a strain contrast of greater than 1, and endometrial polyps have a strain contrast of less than 1. There are a few cases in which this generalization does not fit, such as in the smaller leiomyomas in patient 17. The strain in the leiomyoma is about the same as that in the background, giving a strain contrast equal to or less than 1. This may be due to the age of the leiomyoma and the degree of degeneration of the tissue within it, as well as the size, which is not exactly known. In these cases, the bright slipping artifact surrounding the leiomyoma could be used to distinguish the leiomyoma from the surrounding normal myometrium. More data are needed to investigate the relationship between the strain characteristics, the size of the leiomyoma, and the histologic content of the leiomyoma and the myometrium when there is essentially no strain contrast between the background and the leiomyoma.

Comparison With Mechanical Testing on Excised Uteri

The strain contrast results can be compared to the modulus contrast results[31] determined from dynamic testing of the excised uterine samples used in this study. The modulus contrast is defined as the ratio of the Young's moduli of the 2 regions:

$$\text{modulus contrast} \equiv \frac{\text{Young's modulus lesion}}{\text{Young's modulus background}}.$$

Kiss et al[31] reported that at quasistatic frequencies of 0.1 to 1.0 Hz, the elastic contrast ranges from 2.3 to 3.0 for 2% precompression and 1% dynamic amplitude. This is well within the SD of the mean strain contrast of the large leiomyomas and close to the mean of the contrast of the small leiomyomas (Table 2).

Conclusions

The preliminary results indicate that ultrasound strain imaging does provide differentiation between normal uterine muscle tissue and pathologies such as leiomyomas and endometrial polyps. A uterine leiomyoma may also be distinguished from the normal surrounding myometrium on strain images by the presence of a slipping artifact at the boundary of the leiomyoma. Strain contrast can also differentiate between endometrial polyps and uterine leiomyomas. The strain contrast of a leiomyoma has been shown to be greater than 1, whereas that of an endometrial polyp was less than 1. The strain contrast of leiomyomas was comparable with the modulus contrast values determined by mechanical testing of excised tissue samples.

However, the data presented in this study lacked a leiomyoma protruding into the endometrial cavity or a case in which a leiomyoma and an endometrial polyp were within the same field of view. More data from excised uteri are necessary to obtain a wider variety of leiomyoma sizes and locations, adenomyosis, endometrial polyps, and other conditions to determine the limits of strain imaging in the uterus using ultrasound. It is hoped that uterine strain imaging can provide additional diagnostic information using the same RF data acquired during B-mode ultrasound scanning of the uterus. Potentially, the combination of B-mode and strain imaging of the uterus will allow the physician to make an improved noninvasive diagnosis and to choose the appropriate treatment method.

References

1. Ascher SM, Reinhold C. Imaging of cancer of the endometrium. Radiol Clin North Am 2002; 40:563–576.
2. Bhatia KG, Singh VR. Ultrasonic characteristics of leiomyoma uteri in vitro. Ultrasound Med Biol 2001; 27:983–987.
3. Wood C. Surgical and medical treatment of adenomyosis. Hum Reprod Update 1998; 4:323–326.
4. Williams PL, Laifer-Narin SL, Ragavendra N. Ultrasound of abnormal bleeding. Radiographics 2003; 23:703–718.
5. Davidson KG, Dubinsky TJ. Ultrasonographic evaluation of the endometrium in postmenopausal vaginal bleeding. Radiol Clin North Am 2003; 41:769–780.
6. Devlieger R, D'Hooghe T, Timmerman D. Uterine adenomyosis in the infertility clinic. Human Reprod Update 2003; 9:139–147.

7. Davis PC, O'Neill MJ, Yoder IC, Lee SI, Mueller PR. Sonohysterographic findings of endometrial and subendometrial conditions. Radiographics 2002; 22:803–816.
8. Martínez-Pérez O, Pérez-Medina T, Bajo-Arenas J. Ultrasonography of endometrial polyps. Ultrasound Rev Obstet Gynecol 2003; 3:43–50.
9. Keshavarzi A, Vaezy S, Kaczkowski PJ, et al. Attenuation coefficient and sound speed in human myometrium and uterine fibroid tumors. J Ultrasound Med 2001; 20:473–480.
10. Szabó I. Transvaginal color Doppler for assessment of uterine vascularity in cases of uterine fibroids and sarcomas. Ultrasound Rev Obstet Gynecol 2003; 3:294–299.
11. Berridge DL, Winter TC. Saline infusion sonohysterography: technique, indications, and imaging findings. J Ultrasound Med 2004; 23:97–112.
12. Reinhold C, Tafozoli F, Mehio A, et al. Uterine adenomyosis: endovaginal US and MR imaging features with histopathologic correlation. Radiographics 1999; 19(special issue): S147–S160.
13. Nalaboff KM, Pellerito JS, Ben-Levi E. Imaging the endometrium: disease and normal variants. Radiographics 2001; 21:1409–1424.
14. Reinhold C, McCarthy S, Bret PM, et al. Diffuse adenomyosis: comparison of endovaginal US and MR imaging with histopathologic correlation. Radiology 1996; 199: 151–158.
15. Dueholm M, Lundorf E, Hansen ES, Ledertoug S, Olesen F. Accuracy of magnetic resonance imaging and transvaginal ultrasonography in the diagnosis, mapping, and measurement of uterine myomas. Am J Obstet Gynecol 2002; 186: 409–415.
16. O'Neill MJ. Sonohysterography. Radiol Clin North Am 2003; 41:781–797.
17. Bazot M, Cortez A, Darai E, et al. Ultrasonography compared with magnetic resonance imaging for the diagnosis of adenomyosis: correlation with histopathology. Hum Reprod 2001; 16:2427–2433.
18. Hughes JL, Reidy JF. Imaging and treatment of uterine fibroids including the role of uterine artery embolization. Imaging 2003; 15:79–88.
19. Sierra R, Bajka M, Székely G. Pathology design for surgical training simulators. Lect Notes Comput Sci 2003; 2673:375–384.
20. Garra BS, Cespedes EI, Ophir J, et al. Elastography of breast lesions: initial clinical results. Radiology 1997; 202:79–86.
21. Hall TJ, Zhu Y, Spalding CS. In vivo real-time freehand palpation imaging. Ultrasound Med Biol 2003; 29:427–435.
22. Ophir J, Kallel F, Varghese T, et al. Elastography. CR Acad Sci Paris 2001; 2:1193–1212.
23. Parker KJ, Taylor LS, Gracewski S, Rubens DJ. A unified view of imaging the elastic properties of tissue. J Acoust Soc Am 2005; 117:2705–2712.
24. McCracken PJ, Manduca A, Felmlee J, Ehman RL. Mechanical transient-based magnetic resonance elastography. Magn Reson Med 2005; 53:628–639.
25. McKnight AL, Kugel JL, Rossman PJ, Manduca A, Hartmann LC, Ehman RL. MR elastography of breast cancer: preliminary results. AJR Am J Roentgenol 2002; 178:1411–1417.
26. Ringleb SI, Chen Q, Lake DS, Manduca A, Ehman RL, An KN. Quantitative shear wave magnetic resonance elastography: comparison to a dynamic shear material test. Magn Reson Med 2005; 53:1197–1201.
27. Sinkus R, Tanter M, Catheline S, et al. Imaging anisotropic and viscous properties of breast tissue by magnetic resonance-elastography. Magn Reson Med 2005; 53:372–387.
28. Sinkus R, Tanter M, Xydeas T, Catheline S, Bercoff J, Fink M. Viscoelastic shear properties of in vivo breast lesions measured by MR elastography. Magn Reson Imaging 2005; 23:159–165.
29. Van Houten EEW, Doyley MM, Kennedy FE, Weaver JB, Paulsen KD. Initial in vivo experience with steady-state subzone-based MR elastography of the human breast. J Magn Reson Imaging 2003; 17:72–85.
30. Zhu Y, Hall TJ. A modified block matching method for real-time freehand strain imaging. Ultrason Imaging 2002; 24:161–176.
31. Kiss MZ, Hobson MA, Varghese T, et al. Frequency-dependent complex modulus of the uterus: preliminary results. Phys Med Biol 2006; 51:3683–3695.
32. Konofagou EE, Harrigan T, Ophir J. Shear strain estimation and lesion mobility assessment in elastography. Ultrasonics 2000; 38:400–404.
33. Meixner DD, Hangiandreou NJ, Charboneau JW, et al. Initial clinical experience with real-time ultrasound strain imaging of the thyroid. In: RSNA 2002. Oak Brook, IL: Radiological Society of North America; 2002:713.